Anomalous X-ray scattering study of aqueous solutions of YCl_3 and $ErCl_3$

1990 J. Phys.: Condens. Matter 2 9133

(http://iopscience.iop.org/0953-8984/2/46/013)

J. Phys.: Condens. Matter **2** (1990) 9133–9143. Printed in the UK

Anomalous x-ray scattering study of aqueous solutions of YCl_3 and $ErCl_3$

E Matsubara, K Okuda and Y Waseda
Research Institute of Mineral Dressing and Metallurgy (SENKEN), Tohoku University, Sendai 980, Japan

Received 18 April 1990, in final form 9 July 1990

Abstract. Concentrated (0.1–1.0 kmol m^{-3}) aqueous solutions of YCl_3 and $ErCl_3$ have been studied by the anomalous x-ray scattering (AXS) technique at the Y K-absorption and Er L_{III}-absorption edges, respectively. The Y^{3+} ions are found to have 8.1 ± 0.3 and 8.2 ± 0.5 water molecules with the average Y^{3+}–H_2O distances being 0.246 ± 0.002 and 0.251 ± 0.002 nm for 0.5 and 1.0 kmol m^{-3} YCl_3. Similarly, the Er^{3+} ions are surrounded by 8.2 ± 0.6 and 8.3 ± 0.8 water molecules with the average distances being 0.240 ± 0.002 and 0.238 ± 0.002 nm for 0.5 and 1.0 kmol m^{-3} $ErCl_3$. These results show that the hydration structures around Y^{3+} or Er^{3+} ions in YCl_3 or $ErCl_3$ solutions resemble each other. In the present study, the limit of the concentration of cations applicable to the AXS measurements has also been verified.

1. Introduction

To characterize the atomic structure of aqueous solution is not an easy task using the conventional x-ray diffraction method alone. In a binary metal–halide aqueous solution, for example, the total structure factor comprises ten partial structure factors. Even if the contribution of hydrogen atoms to scattering intensity is ignored because of its very small scattering power for x-rays, there are still six partial structure factors. Thus, separating the individual contributions of such components is very difficult and sometimes involves some uncertain assumptions.

The anomalous x-ray scattering (AXS) method used in the present study prevails over these difficulties since it provides the chemical selectivity to determine the environmental radial distribution function (RDF) around a specific constituent element. While the energy-derivative method has been adopted in the present AXS method, its basic concept was proposed by Hosoya [1] and Shevchik [2] and it was first used by Fuoss *et al* [3] with synchrotron radiation under the name of differential anomalous scattering (DAS). The structural study of the concentrated aqueous solutions of several bromides by Ludwig and his colleagues [4] demonstrated that the AXS method is a powerful tool for investigating the hydration of aqueous solution. In a recent publication [5], we discussed the hydration of Zn^{2+} ions in 0.98 and 2.85 kmol m^{-3} $ZnCl_2$ aqueous solutions using this AXS method. This method is analogous to the isotope substitution method in neutron scattering which has successfully been applied in several solutions, such as $NiCl_2$ in aqueous solution [6]. The structure is automatically assumed to remain identical upon

0953-8984/90/469133 + 11 $03.50

substitution by the isotope including the use of deuterium, but this assumption may be valid in a thermodynamically equilibrated liquid state. Note also that the relative change in scattering intensity in the isotope substitution method is larger than that in the AXS method. The extended x-ray absorption fine structure (EXAFS) technique, which also has chemical selectivity, is quite effective in determining local atomic arrangements around a specific element at the nearest-neighbour distance. However, there is some theoretical ambiguity in the determination of some parameters used in the EXAFS analysis, such as determination of back amplitudes and phase shifts (for example, see [7]). This is particularly true in the EXAFS analysis of disordered systems.

Few studies in aqueous solutions of some salts of rare-earth elements are available in comparison with those of divalent transition metals. Since the rare-earth elements are trivalent and large ions in solutions, it is expected that hydration numbers are quite large. Habenschuss and Spedding [8] systematically studied the concentrated chloride aqueous solutions of the lanthanide elements using the ordinary x-ray diffraction technique and reported an average hydration number of nine for the ions of the light rare-earth elements and of eight for the ions of the heavy rare-earth elements (those between Nd^{3+} and Tb^{3+} are transitional). Narten and Hahn [9] studied the hydration of Nd^{3+} and Cl^- ions in 2.85 kmol m^{-3} D_2O solutions of $NdCl_3$ by neutron scattering from isotopically substituted samples and determined that the Nd^{3+} ion is surrounded by 8.5 water molecules. Similarly, information on the hydration of the Dy^{3+} ion was discussed by neutron diffraction and it was found that each Dy^{3+} ion is surrounded by 7.4 water molecules [10]. In a recent study of Dy^{3+} and Yb^{3+} aqueous solutions using the neutron diffraction difference technique [11], it was found that Dy^{3+} and Yb^{3+} ions are surrounded by 7.9 and 7.8 water molecules at 0.239 ± 0.002 and 0.233 ± 0.002 nm, respectively.

To the best of our knowledge, structural studies of aqueous solution of YCl_3 by any diffraction technique have not been reported. In the present study, we have used the AXS method to discuss the hydration of a Y^{3+} ion in 0.1, 0.5 and 1.0 kmol m^{-3} aqueous solutions of YCl_3. It is well known that the extraction behaviour of Y with respect to the 2-ethyl-hexyl phosphoric acid (D2EHPA) which is one of the most commonly used extractants in practice lies between those of Ho and Er [12]. Thus, it is likely that some kind of similarity might also be quite realistic in the hydration of the Y^{3+} and Er^{3+} ions. For a comparison, 0.1, 0.5 and 1.0 kmol m^{-3} aqueous solutions of $ErCl_3$ were also measured.

2. Experimental procedure

Aqueous solutions of YCl_3 and $ErCl_3$ were prepared by dissolving crystals in deionized water. Exact 0.10, 0.50 and 1.00 kmol m^{-3} solutions of each chloride were prepared, their concentrations being carefully controlled using EDTA (ethylene-diaminetetraacetic acid) titration, with xylenol orange as the indicator. Densities of each solution determined with a pycnometer are summarized in table 1.

Scattering data were collected at the Photon Factory of the National Laboratory for High-Energy Physics, Tsukuba, Japan, using the beam line 6B where a double Si (111) crystal monochromator is installed. The details of the experimental apparatus are described in [13]. Some additional details necessary for the present study are given below. Because of particular near-edge phenomena, such as x-ray absorption near-edge structure (XANES) and EXAFS, and extremely intense fluorescent radiation above the

Table 1. Compositions and densities of the aqueous solutions used in the present measurements.

YCl_3 (kmol m^{-3})	Y (at.%)	Cl (at.%)	H (at.%)	O (at.%)	Density (10^3 kg m^{-3})
0.1	0.06	0.18	66.51	33.25	1.020
0.5	0.30	0.90	65.87	32.93	1.088
1.0	0.60	1.80	65.07	32.53	1.172
$ErCl_3$ (kmol m^{-3})	Er (at.%)	Cl (at.%)	H (at.%)	O (at.%)	Density (10^3 kg m^{-3})
0.1	0.06	0.18	66.51	33.25	1.025
0.5	0.30	0.90	65.87	32.93	1.128
1.0	0.60	1.80	65.07	32.53	1.251

absorption edge, AXS data for Y and Er were collected at the energies below Y K- and Er L_{III}-absorption edges, respectively. The intensity of the incident beam was monitored by a nitrogen-gas flow type ion chamber placed in front of the samples. Observed intensities were converted to intensity in counts per photon by dividing the total number of photons calculated from the monitor counts [14]. A portable pure germanium solid-state detector was used to ensure that the sum of coherent and incoherent intensities, and Y Kα from the solutions of YCl_3 were separately collected. The Y Kβ fluorescence overlapping with these coherent and incoherent intensities near the Y K-absorption edge was corrected [15] by subtracting the intensity of the Kβ fluorescence estimated from the measured intensity of the Kα fluorescence and the intensity ratio of Kβ to Kα [16]. Similarly, Er Lα fluorescence from the solutions of $ErCl_3$ was separately collected and used with the intensity ratio of Lβ to Lα [17] to correct for the Er Lβ fluorescence overlapping with the coherent and incoherent scattering near the Er L_{III}-absorption edge. In the measurements of the $ErCl_3$ solutions, the effect of higher harmonics diffracted by a Si (333) was reduced to an insignificant level by intentionally detuning the second crystal of the monochromator with a piezoelectric device attached to it. Escape peaks of the coherent and Y Kα fluorescent radiations were observed in the measurements of the YCl_3 solutions because of a germanium single crystal in the detector. Their intensities were monitored and added to those of the original coherent and fluorescent intensities, respectively.

Scattering intensities from the solutions were collected using two different geometries, namely symmetrical reflection and transmission geometries. A cell of 12 mm depth covered with a window of a thin 'kapton' film was used for the measurements in the reflection geometry. Incidentally, this kapton film shows a relatively sharp peak at about 4 nm^{-1}. In the reflection geometry, the contribution of scattering intensity from the window becomes very large at low scattering angles, which sometimes disturbs the accurate measurement of scattering intensity from the sample itself. Thus, intensity at the low angular region was also measured in the transmission geometry, using a cell confined between thin kapton films. The contributions from the window of 25 μm thickness in the 0.1, 0.5 and 1.0 kmol m^{-3} YCl_3 solutions were at most 12, 7.8 and 6.3% in the transmission geometry and 4.3, 5.1 and 5.8% in the reflection geometry, respectively. The values for the 0.1, 0.5 and 1.0 kmol m^{-3} $ErCl_3$ solutions were at most

19, 6.0 and 3.3% in the transmission geometry and 14, 16 and 18% in the reflection geometry. The larger contributions from the window in the $ErCl_3$ solutions are explained by the lower incident beam energies used for the AXS measurements below the Er L_{III}-absorption edge. Correction for the scattering by the window of the cell in each geometry was made by separately measuring the intensities from the empty cell (I_c) and the filled cell (I_s), and in the usual manner already described in [5]. The products of thicknesses and linear absorption coefficients for the sample and kapton film appearing in this correction were experimentally estimated from the absorption by the filled and empty cells in each solution [5]. The corrected intensities in both geometries were combined for further analyses of the data.

The minimum total counts collected at each scattering angle was about 70 000 counts, the average being about more than 120 000 counts in each solution of YCl_3. On the other hand, because of the large absorption coefficients of the samples at Er L_{III} absorption edge, the total counts observed in each solution of $ErCl_3$ were much less than those of YCl_3. The minimum number of counts collected was about 20 000, the average being about 60 000 counts. However, it may be added that the energy dependence is rather clearly detected due to the larger variation of f' of Er at the L_{III}-absorption edge. The corrected intensity was converted to electron units per atom by the generalized Krogh–Moe–Norman method [18], using the x-ray atomic scattering factors of Y^{3+}, Er^{3+}, Cl^-, H and O [19], including their anomalous dispersion terms [20] theoretically calculated by the method of Cromer and Liberman [21], and Compton scattering factors of Y, Er, Cl and O from [22] and H from [23] with so-called Breit–Dirac recoil factors. The variation of the anomalous dispersion term below the absorption edge depending on the valence state appears to be negligibly small although its value above the edge frequently changes due to the XANES [24]. Thus, for the anomalous dispersion terms of Y^{3+} and Er^{3+} ions, the values of the neutral atoms of Y and Er were used in this work where only the energies in the lower energy side of the edge were employed. In the present study, intensity data at Q values less than 2.5 nm^{-1} have been smoothly extrapolated to Q = 0 nm^{-1}. The effect of the extrapolation and the truncation up to 110 nm^{-1} for the YCl_3 solutions and 75 nm^{-1} for the $ErCl_3$ solutions is known to give no critical alteration in the RDF calculated by Fourier transformation [25, 26]. However, it is relatively easy to trace the positions where the spurious ripples due to the limited termination become significant. For example, the oscillations of such ripples appear at $r = \pm 5\pi/2Q_{max}$ or $\pm 9\pi/2Q_{max}$ from the position of the principal peak where Q_{max} is the upper limit used in the experiment, following the works of Finbak [27] and Morimoto [25]. Thus, the locations of these ripples, if any, are estimated to be 0.12, 0.20, 0.41 and 0.49 nm for the Y^{3+} aqueous solutions and 0.17, 0.23, 0.37 and 0.43 nm for the Er^{3+} aqueous solutions. The coincidence between the experimental data and the estimated positions in oscillations was not quantitatively confirmed in the 0.5 and 1.0 kmol m^{-3} YCl_3 and $ErCl_3$ solutions. However, it may be noted that a couple of weak ripples in the 0.1 kmol m^{-3} YCl_3 and $ErCl_3$ solutions are located at the corresponding distances estimated here. This suggests some reservations regarding the quantitative accuracy of RDFs for the 0.1 kmol m^{-3} YCl_3 and $ErCl_3$ solutions, which will be considered later.

When the incident beam energy is selected at the lower energy side of the absorption edge of the jth element, the variation detected in the scattering intensity is attributed only to the change of the real part of the anomalous dispersion term f' of the jth element. Thus, the difference between scattering intensities measured at two energies E_1 and E_2 ($E_1 < E_2$) is given by

$$\Delta i(Q) = \left(I_{eu}^{coh}(Q, E_1) - \sum_{k=1}^{n} c_k f_k^2(Q, E_1)\right) - \left(I_{eu}^{coh}(Q, E_2) - \sum_{k=1}^{n} c_k f_k^2(Q, E_2)\right) \quad (1)$$

where n is the number of the constituent elements, and f_k and c_k are the scattering factor and concentration of the kth element, respectively. The environmental reduced RDF around the jth element, $G_j(r)$, is determined by the Fourier transform of the quantity $Q\Delta i(Q)$:

$$G_j(r) = \frac{2}{\pi c_j (f_j'(E_1) - f_j'(E_2))} \int_0^\infty \frac{Q\Delta i(Q) \sin(Qr)}{W(Q)} \, dQ \quad (2)$$

and

$$W(Q) = \sum_{k=1}^{n} c_k \, \mathrm{Re}(f_k(Q, E_1) + f_k(Q, E_2)). \quad (3)$$

The function $G_j(r)$ is also given by a sum of the reduced partial RDFs $g_{jk}(r)$. Namely, in the YCl_3 aqueous solution, the function $G_Y(r)$ is given as a sum of the four partial RDFs:

$$G_Y(r) + 4\pi r\rho_0 = g_{YO}(r) + g_{YH}(r) + g_{YCl}(r) + g_{YY}(r) \quad (4)$$

where ρ_0 is the average number density. These reduced partial RDFs are described with the number density of the constituent elements around Y, $\rho_{Yk}(r)$. Namely,

$$g_{Yk}(r) = 4\pi r \frac{\mathrm{Re}(f_k(Q, E_1) + f_k(Q, E_2))}{W(Q)} \rho_{Yk}(r). \quad (5)$$

Consequently, the left-hand side of (4) is described, in the following, as a sum of the four partial number densities $\rho_{Yk}(r)$

$$4\pi r(A\rho_{YO}(r) + B\rho_{YH}(r) + C\rho_{YCl}(r) + D\rho_{YY}(r)). \quad (6)$$

The equations for the $ErCl_3$ solutions are also obtained by replacing the subscripts of Y in (4) to (6) with Er. The values of the sample parameters, A, B, C and D for each solution of YCl_3 and $ErCl_3$ are given in table 2, using the average values of the scattering factors in the measured regions ($2.5\,nm^{-1} \leq Q \leq 110\,nm^{-1}$ for the YCl_3 and $2.5\,nm^{-1} \leq Q \leq 75\,nm^{-1}$ for the $ErCl_3$).

Table 2. Sample parameters denoted by (6) for the aqueous solutions of 0.1, 0.5 and 1.0 kmol m^{-3} YCl_3 and $ErCl_3$.

		A	*B*	*C*	*D*
YCl_3	0.10	2.65	0.145	7.67	14.9
	0.50	2.45	0.136	7.07	13.7
	1.00	2.24	0.126	6.43	12.5
$ErCl_3$	0.10	2.52	0.205	6.55	22.1
	0.50	2.31	0.190	5.98	20.2
	1.00	2.09	0.173	5.40	18.2

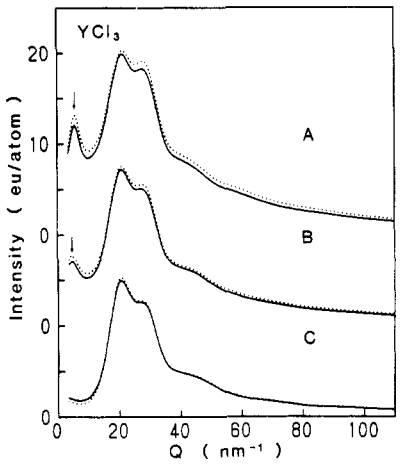

Figure 1. Intensity profiles (I_{eu}^{coh}) measured at 17.013 (——) and 16.737 (· · · ·) keV for the aqueous solutions 1.0 (curves A), 0.5 (curves B) and 0.1 (curves C) kmol m^{-3} YCl_3. Arrows indicate prepeaks.

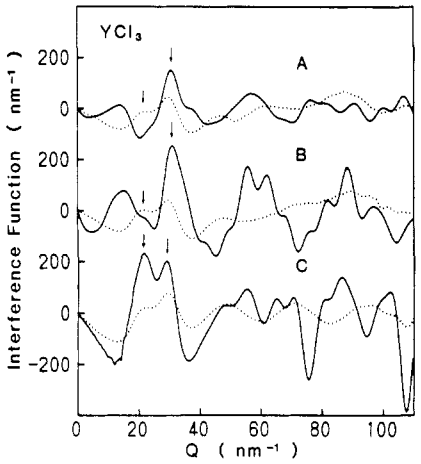

Figure 2. Differential interference functions $Q\Delta i(Q)$ (——) and interference functions $Qi(Q)$ (· · · ·) for the aqueous solutions of 1.0 (curves A), 0.5 (curves B) and 0.1 (curves C) kmol m^{-3} YCl_3. The functions of $Qi(Q)$ in the figure are multiplied by four and the function of $Q\Delta i(Q)$ in C is divided by three.

The ordinary reduced RDFs $G(r)$ were also estimated in each solution of YCl_3 and $ErCl_3$, using the coherent intensities in electron units per atom, $I_{eu}^{coh}(Q)$ determined at the lower energy below each absorption edge. The essential equations are as follows

$$G(r) = \frac{2}{\pi}\int_0^\infty Qi(Q)\sin(Qr)\,\mathrm{d}Q \tag{7}$$

and

$$i(Q) = \left(I_{eu}^{coh}(Q) - \sum_{k=1}^{n} c_k f_k^2\right) \Big/ \left(\sum_{k=1}^{n} c_k f_k\right)^2. \tag{8}$$

3. Results and discussion

Coherent intensity profiles (I_{eu}^{coh}) of the 1.0, 0.5 and 0.1 kmol m^{-3} YCl_3 aqueous solutions are shown in figure 1. The full and dotted curves of each solution describe the scattering intensities at 17.013 and 16.737 keV, respectively. Each energy corresponds to energies of 25 and 301 eV below the Y K absorption edge (17.038 keV). These profiles essentially show typical profiles of aqueous solutions containing metallic ions, having a broad first peak at about 20 nm^{-1} with a shoulder at about 28 nm^{-1}. In addition to these ordinary features, there is a prepeak whose intensity and position increase with YCl_3 concentrations. This implies that the prepeak is closely associated with some pairs relating with the Y^{3+} and/or Cl^- ions. The presence of a similar prepeak has already been reported in some concentrated aqueous solutions such as $NiCl_2$ [6] and $ZnCl_2$ [5]. Nevertheless, in order to understand the origin of the prepeak, a further structural analysis similar to

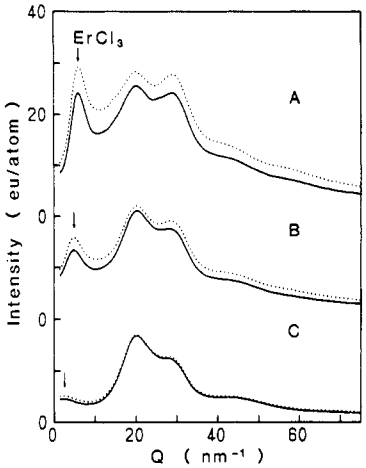

Figure 3. Intensity profiles (I_{eu}^{coh}) measured at 8.339 (——) and 8.064 (· · · ·) keV for the aqueous solutions 1.0 (curves A), 0.5 (curves B) and 0.1 (curves C) kmol m^{-3} $ErCl_3$. Arrows indicate prepeaks.

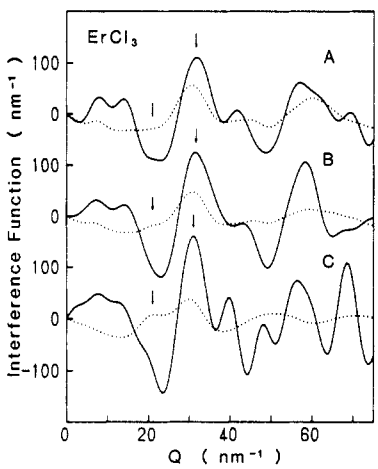

Figure 4. Differential interference functions $Q\Delta i(Q)$ (——) and interference functions $Qi(Q)$ (· · · ·) for the aqueous solutions of 1.0 (curves A), 0.5 (curves B) and 0.1 (curves C) kmol m^{-3} $ErCl_3$. The functions of $Qi(Q)$ in the figure are multiplied by two and the function of $Q\Delta i(Q)$ in C is divided by two.

that in [28] using the method of multi-pattern analysis is required by neutron diffraction from isotopically enriched samples. Such an experiment is an important future subject for the structure of various electrolytic solutions.

The differential interference functions in (1) multiplied by Q, $Q\Delta i(Q)$ of the YCl_3 solutions are shown in figure 2, with the ordinary interference function $Qi(Q)$ obtained in a similar manner to the function $i(Q)$ in (8). The $Q\Delta i(Q)$ functions of 1.0 and 0.5 kmol m^{-3} YCl_3 solutions have no peak at the positions of the first peak of $Qi(Q)$ although the peaks at 28 nm^{-1} are present in both $Q\Delta i(Q)$ and $Qi(Q)$. However, this is not the case in the 0.1 kmol m^{-3} YCl_3 solution. Both the first peak and its shoulder exist even in $Q\Delta i(Q)$. The intensity differences at the shoulder of the first peak for the 1.0 and 0.5 kmol m^{-3} solutions are, for example, about 5.8 and 4.0%, this difference for the 0.1 kmol m^{-3} solution being about 1.6%. The experimental error due to the counting statistics, the uncertainties of mass absorption coefficients and anomalous dispersion terms caused by the finite energy resolution of the incident beam (which is about 7 eV in the present study), the errors of densities and concentrations of the solutions, and so on, whose relative magnitudes are about 0.3, 0.4 and 0.2%, respectively, is estimated to be about 1%. Thus, it is predicted that the determination of the environmental structure around Y in the 0.1 kmol m^{-3} YCl_3 solution is quite demanding in the present experiment.

Similar behaviour of the prepeaks is also observed in the scattering intensity profile of the $ErCl_3$ solutions in figure 3. The full and dotted curves of each solution represent the scattering intensities at 8.339 and 8.064 keV, respectively, which correspond to 18.5 and 293.5 eV below the Er L_{III}-absorption edge (8.3575 keV). The relative intensity of the prepeak is much larger in the $ErCl_3$ solution than that in the YCl_3 solution. The relatively distinct prepeak in the $ErCl_3$ solutions is qualitatively understood by the fact that the scattering intensity of Er is about three times larger than that of Y.

The magnitude of the real part of the anomalous dispersion term f' near the L_{III}-absorption edge is about three times larger than that near the K-absorption edge and the amount of change of f' is must larger near the L_{III}-absorption edge than near the K-absorption edge. Incidentally, the difference of the f' for Er at the two incident beam energies used for the present AXS measurements below the Er L_{III}-absorption edge is 5.87, that for Y at the two energies below the Y K-absorption edge being 2.41. Therefore, the intensity difference in the $ErCl_3$ solutions becomes larger than that in the YCl_3 solutions. The intensity differences at the shoulder of the first peak in 1.0, 0.5 and 0.1 kmol m^{-3} $ErCl_3$ solutions are about 14.8, 9.4 and 3.9%, respectively. These values are more than twice as much as those in the YCl_3 solutions. $Q\Delta i(Q)$ and $Qi(Q)$ for the $ErCl_3$ solutions are shown in figure 4. As observed in figure 2, the first peak at about 20 nm^{-1} of $Qi(Q)$ disappears in $Q\Delta i(Q)$ and its shoulder is magnified by taking the difference. The same pattern at the first peak is observed even in the lowest molar concentration of $ErCl_3$ although $Q\Delta i(Q)$ in the 0.1 kmol m^{-3} YCl_3 solution does not give the appropriate differential intensity profile. This is easily understood by the larger difference of f' at the Er L_{III}-absorption edge. A close look at each differential profile of the $ErCl_3$ solutions reveals that $Q\Delta i(Q)$ in the high Q region in the 0.1 kmol m^{-3} $ErCl_3$ solution is slightly different from the others, which may cause a disagreement in the environmental RDF of the 0.1 kmol m^{-3} $ErCl_3$ solution with the others.

Environmental reduced RDFs around Y, $G_Y(r)$ for each YCl_3 solution determined by Fourier transformation of the differential interference functions $Q\Delta i(Q)$ in (2) are shown in figure 5, with the ordinary reduced RDFs $G(r)$ obtained in a similar manner to the function $Qi(Q)$ in (7). Three peaks at 0.246 ± 0.002, 0.306 ± 0.002 and 0.357 ± 0.002 nm indicated by arrows in the figure are observed in the nearest-neighbour region of $G(r)$ of the 1.0 kmol m^{-3} YCl_3 solution. The first peak in $G(r)$ is attributed to the pairs of Y^{3+} and O of the water molecule since it shows a peak even in $G_Y(r)$. In the present AXS measurements, more than 90% of the total contribution is attributed to the pairs of Y^{3+} and O of the water molecule in the nearest-neighbour region around hydrogenated Y ions. Thus, by assuming only the Y^{3+} and O pairing, the hydration number of Y^{3+} was calculated from the area under the first peak of $G_Y(r)$. It is known that no unique procedure is available, at the present time, for estimating the experimental uncertainty of the coordination number calculated from the RDF data. Thus, the error in the coordination number due to counting statistics was estimated from the variance of the function $G_Y(r)$, $\sigma[G_Y(r)]$, which is given by [29]

$$\sigma^2[G_Y(r)] = \left(\frac{2}{\pi c_Y(f'_Y(E_1) - f'_Y(E_2))}\right)^2 \int_0^\infty \frac{Q^2\sigma^2[\Delta i(Q)]\exp(-2\alpha^2Q^2)}{W(Q)^2}(\sin Qr)^2\,\mathrm{d}Q. \tag{9}$$

The variance of $\Delta i(Q)$ can be readily obtained from the counting statistical error in the intensity. This counting error was evaluated using the equation of the probable error defined by Cullity [30]. The resultant values in each solution of YCl_3 are summarized in table 3. The following comments may be made, regarding the error in the coordination number. A source of systematic errors in liquid structure by x-ray diffraction arises from the uncertainties in the atomic scattering factors and in the Compton scattering. According to the detailed discussion given in [31], the maximum error in these quantities is estimated to be less than 1% for the constituent elements investigated here. Therefore, the total experimental uncertainty of the coordination number calculated in this work does not exceed the variation due to the counting statistics given in table 3.

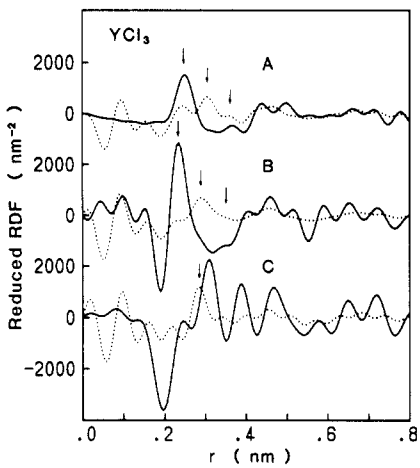

Figure 5. Environmental reduced radial distribution functions (RDFs) around the Y^{3+}, $G_Y(r)$ (——) and ordinary reduced RDFs $G(r)$ (· · · ·) for the aqueous solutions of 1.0 (curves A), 0.5 (curves B) and 0.1 (curves C) kmol m^{-3} YCl_3. Arrows indicate the three peaks in the nearest-neighbour region. The first peak of $G_Y(r)$ indicated by the arrow was used for computation of the hydration numbers. The ordinary RDFs in the figure are multiplied by four and the environmental RDF in C is divided by three.

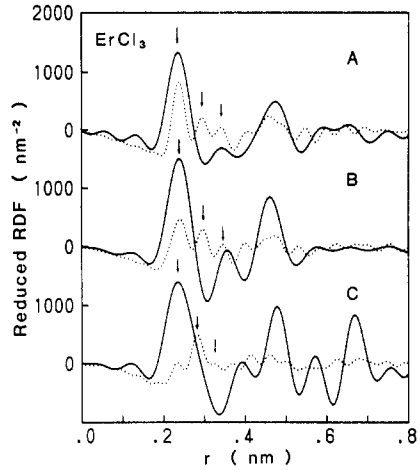

Figure 6. Environmental reduced radial distribution functions (RDFs) around the Er^{3+}, $G_{Er}(r)$ (——) and ordinary reduced RDFs $G(r)$ (· · · ·) for the aqueous solutions of 1.0 (curves A), 0.5 (curves B) and 0.1 (curves C) kmol m^{-3} $ErCl_3$. Arrows indicate the three peaks in the nearest-neighbour region. The first peak of $G_{Er}(r)$ indicated by the arrow was used for computation of the hydration numbers. The ordinary RDFs in the figure are multiplied by two and the environmental RDF in C is divided by two.

Table 3. Summary of hydration numbers (N) and distance (r) in the concentrated aqueous solutions of YCl_3 and $ErCl_3$.

Salts	Molarity (kmol m^{-3})	r (nm)	N
YCl_3	1.0	0.251 ± 0.002	8.2 ± 0.5
	0.5	0.246 ± 0.002	8.1 ± 0.3
$ErCl_3$	1.0	0.238 ± 0.002	8.3 ± 0.8
	0.5	0.240 ± 0.002	8.2 ± 0.6

The position of the second peak in $G(r)$ shifts to lower r with a decrease in the concentration of YCl_3, i.e. 0.306 ± 0.002, 0.289 ± 0.002 and 0.286 ± 0.002 nm for 1.0, 0.5 and 0.1 kmol m^{-3} YCl_3 solutions, respectively, and approaches the value of the O–O distance of pure liquid water, 0.285 nm [32]. Thus, this second peak is assigned to the O–O pairs and the slight shift of the peak position at the higher concentration is ascribed to the overlap of the first peak of the Y^{3+}–O pairs. Biggin *et al* [33] studied the hydration of Cl^- ion in a 2.85 kmol m^{-3} $NdCl_3$ in D_2O solution with the isotope substitution technique by neutron diffraction. According to their results, the distance between Cl^- and O of D_2O molecules is 0.345 ± 0.004 nm. Thus, the third peak at about 0.355 nm in

the 1.0 kmol m^{-3} YCl_3 solution may result mainly from the Cl^-–O pairs, which is consistent with the fact that this peak almost disappears by taking the difference. However, a small peak still exists in $G_Y(r)$. The presence of this small peak in $G_Y(r)$ at the third peak position of $G(r)$ might suggest the presence of a small amount of such second-nearest-neighbour water molecules in concentrated aqueous solutions. In the 0.1 kmol m^{-3} YCl_3 solutions, a peak for the Y^{3+}–O pairing is not clearly observed and a peak for O–O pairs is still present in the $G_Y(r)$ curve. As discussed in the differential intensity profiles, the magnitude of the experimental error is almost comparable to the intensity difference. Therefore, the accuracy of the intensity difference determined by the energy derivative method is not good enough to estimate the correct $G(r)$. In other words, the AXS method cannot be applied to such a dilute solution of YCl_3 in the present experimental conditions.

Similarly, $G_{Er}(r)$ and $G(r)$ determined by Fourier transformation of the $Q\Delta i(Q)$ and $Qi(Q)$ in $ErCl_3$ solutions are shown in figure 6. As observed in the YCl_3 solutions, the three peaks are observed in the nearest-neighbour region, and by taking the difference, a large peak and a small peak are left at the positions of the first and third peaks of $G(r)$, the second peak of $G(r)$ disappearing in $G_{Er}(r)$. Therefore, the former two peaks of $G_{Er}(r)$ and $G(r)$ are assigned to Er^{3+}–O and O–O pairs in the same manner as those in the YCl_3 solutions. The hydration numbers of Er^{3+} estimated from the first peak of the $G_{Er}(r)$ are also summarized in table 3 with their errors due to counting statistics and their distances in the 1.0 and 0.5 kmol m^{-3} $ErCl_3$ solutions. On the other hand, the coordination number of the 0.1 kmol m^{-3} $ErCl_3$ solution was estimated to be 10.4. This value is much larger than those for the 0.5 and 1.0 kmol m^{-3} $ErCl_3$ solutions. The first peak of $G_{Er}(r)$ for the 0.1 kmol m^{-3} $ErCl_3$ solution is also found to have a right-skewed nature. In other words, the high-r tail overlaps with the positions of the O–O pairs, which indicates that the environmental RDF around Er^{3+} cannot be determined accurately in this dilute solution. Consequently, it is found that because of the larger difference of f' at the L_{III}-absorption edge, the plausible pattern was obtained even in the 0.1 kmol m^{-3} $ErCl_3$ solution. However, the authors maintain the view that the case of lower concentration was not good enough for quantitative analysis.

In conclusion, both Y^{3+} and Er^{3+} are coordinated by about 8.2 water molecules in solutions of concentrations up to 1 kmol m^{-3} YCl_3 and $ErCl_3$, and the essential configuration around Y^{3+} and Er^{3+} does not show any significant difference in the two solutions. It should also be noted that the presence of some kind of order introduced into the structure around Y^{3+} or Er^{3+} is not completely excluded by the present study since there is a small peak at about 0.35 nm in the environmental reduced RDFs around Y^{3+} or Er^{3+}. The potential capability of the AXS technique to investigate the structure around ions of the heavy rare-earth elements in aqueous solutions has been clearly demonstrated. We believe that the AXS technique is very promising for structural characterization of the concentrated aqueous solution. The applicable limit of this AXS technique to the dilute aqueous solution was found to be the solute concentration of about 0.5 kmol m^{-3} YCl_3 and $ErCl_3$ solutions.

Acknowledgments

Two authors (EM and YW) particularly wish to thank the staff of the Photon Factory, National Laboratory for High Energy Physics, Dr M Nomura and Dr A Koyama.

Professor Y Awakura and Dr T Hirato in Kyoto University provided valuable advice and assistance for the sample preparation.

References

[1] Hosoya S 1970 *Bull. Phys. Soc. Japan* **25** 110
[2] Shevchik N J 1977 *Phil. Mag.* **35** 805
[3] Fuoss P H, Eisenberger P, Warburton W K and Biedenstock A 1981 *Phys. Rev. Lett.* **46** 1537
[4] Ludwig K F Jr, Warburton W K and Fontaine A 1986 *J. Chem. Phys.* **87** 620
[5] Matsubara E and Waseda Y 1989 *J. Phys: Condens. Matter* **1** 8575
[6] Enderby J E, Cummings S, Herdman G J, Neilson G W, Salmon P S and Skipper N 1987 *J. Phys. Chem.* **91** 5851
[7] Lee P A, Citrin P H, Eisenberger P and Kincaid B M 1981 *Rev. Mod. Phys.* **53** 761
[8] Habenschuss A and Spedding F H 1979 *J. Chem. Phys.* **70** 2797, 3758; 1980 *J. Chem. Phys.* **73** 442
[9] Narten A H and Hahn R L 1983 *J. Phys. Chem.* **87** 3193
[10] Annis B K, Hahn R L and Narten A H 1985 *J. Chem. Phys.* **82** 2086
[11] Cossy C, Barnes A C, Enderby J E and Merbach A E 1989 *J. Chem. Phys.* **90** 3254
[12] Peppard D F, Mason G W, Maier J L and Driscoll W J 1957 *J. Inorg. Nucl. Chem.* **4** 334
[13] Waseda Y, Matsubara E and Sugiyama K 1988 *Sci. Rep. Res. Inst. Tohoku Univ.* A **34** 1
[14] Matsubara E, Waseda Y, Mitera M and Masumoto T 1988 *Trans. Japan Inst. Metals* **29** 697
[15] Aur S, Kofalt D, Waseda Y, Egami T, Wang R, Chen H S and Teo B K 1983 *Solid State Commun.* **48** 111
[16] Rao N V, Reddy S B, Satyanarayana G and Sastry D L 1986 *Physica* C **138** 215
[17] Teo B K 1986 *EXAFS: Basic Principles and Data Analysis* (Berlin: Springer) p 15
[18] Wagner C N J, Ocken H and Joshi M L 1965 *Z. Naturf.* a **20** 325
[19] *International Tables for X-ray Crystallography* 1974 vol IV (Birmingham: Kynoch) p 99
[20] Waseda Y 1984 *Novel Application of Anomalous X-ray Scattering for Structural Characterization of Disordered Materials* (New York: Springer) p 84
[21] Cromer D T and Liberman D 1970 *J. Chem. Phys.* **53** 1891
[22] Cromer D T 1969 *J. Chem. Phys.* **50** 4857
[23] Compton A H and Allison S K 1967 *X-rays in Theory and Experiment* 2nd edn (Tront: Van Nostrand) p 782
[24] Petian J and Calas G 1983 *EXAFS and Near Edge Structure* ed A Beanconi, L Incoccia and S Stipcich (Berlin: Springer) p 144
[25] Morimoto H 1958 *J. Phys. Soc. Japan* **13** 1015
[26] Furukawa K 1962 *Rep. Prog. Phys.* **25** 395
[27] Finbak C 1949 *Acta Chem. Scand.* **3** 1279, 1293
[28] Neilson G W and Enderby J E 1983 *Proc. R. Soc.* A **390** 353
[29] Matsubara E, Waseda Y, Ashizuka M and Ishida E 1988 *J. Non-Cryst. Solids* **103** 117
[30] Cullity B D 1978 *Elements of X-ray Diffraction* (Reading, MA: Addison-Wesley) p 220
[31] Greenfield A J, Wellendarf J and Wiser N 1971 *Phys. Rev.* A **4** 1607
[32] Narten A H and Levy H A 1969 *Science* **165** 447
[33] Biggin S, Enderby J E, Hahn R L and Narten A H 1984 *J. Phys. Chem.* **88** 3634